INTERNATIONAL JOURNAL FOR NUMERICAL METHODS IN FLUIDS
Int. J. Numer. Meth. Fluids 2004; **46**:903–920
Published online 17 September 2004 in Wiley InterScience (www.interscience.wiley.com). DOI: 10.1002/fld.788

Comparative study of lattice-Boltzmann and finite volume methods for the simulation of laminar flow through a 4:1 planar contraction

Yarub Y. Al-Jahmany*,†, Gunther Brenner‡ and Peter O. Brunn

Institute of Fluid Mechanics (LSTM), University of Erlangen-Nuremberg, Cauerstrasse 4, D-91058 Erlangen, Germany

SUMMARY

In the present paper, a comparative study of numerical solutions for Newtonian fluids based on the lattice-Boltzmann method (LBM) and the classical finite volume method (FVM) is presented for the laminar flow through a 4:1 planar contraction at a Reynolds number of value one, $Re = 1$. In this study, the stress field for LBM is directly obtained from the distribution function. The calculations of the stress based on the FVM-data use the evaluations of velocity gradients with finite differences. The stress field for both LBM and FVM is expressed in the present study in terms of the shear stress and the first normal stress difference. The lateral and axial profiles of the velocity, the shear stress and the first normal stress difference for both methods are investigated. It is shown that the LBM results for the velocity and the stresses are in excellent agreement with the FVM results. Copyright © 2004 John Wiley & Sons, Ltd.

KEY WORDS: lattice-Boltzmann method; finite volume method; Newtonian fluid; planar contraction; velocity profile; stress distribution

1. INTRODUCTION

It is a well known fact that due to the continuous increase of the performance of computer hardware as well as numerical algorithms, the numerical simulation of fluid flows has developed as a standard tool in engineering and scientific applications. However, with the increasing possibilities of Computational Fluid Dynamics (CFD), the expectations with respect to accuracy and efficiency of these numerical simulations increase too. This has motivated the development of numerous new computational techniques that allow to circumvent many of the inherent deficiencies of the classical CFD methods such as the finite volume/element meth-

*Correspondence to: Y. Y. Al-Jahmany, Institute of Fluid Mechanics (LSTM), University of Erlangen-Nuremberg, Cauerstrasse 4, D-91058 Erlangen, Germany.
†E-mail: jahmany@lstm.uni-erlangen.de
‡Present address: ITM, TU-Clausthal, Graupenstr. 3, D-38678 Clausthal-Zellerfeld, Germany.

Contract/grant sponsor: German Academic Exchange Service DAAD; contract/grant number: Ref. 425

Received 3 June 2003
Revised 19 June 2004

ods to approximate the Navier–Stokes equations. In that context, the lattice-Boltzmann method (LBM) has received much attention as a conceptionally new and promising way in simulating fluid flows. The basic concept goes back to the cellular automata applied to model simplified dynamics of propagation and collisions of fictitious fluid particles [1]. Several conceptual draw backs of this approach have led to the development of the lattice-Boltzmann methods, as presented e.g. in References [2, 3]. The fundamental idea of the LBM is to construct a simplified kinetic models that incorporate the essential physics of microscopic processes so that the averaged properties obey the desired macroscopic equations. The LBM is a relaxation scheme applied to the velocity discrete Boltzmann equation. In that, it represents an approximation of the BGK-equation [4], where the collision integral in the original Boltzmann equation is replaced by a relaxation term without violating the H-theorem. It can be shown that, with suitable linearizations, this approach leads to an approximation of the Navier–Stokes equations in the limit of low Mach number [5]. The advantage of the LBM compared to the 'classical' finite approximations used in fluid dynamics (e.g. finite volume/element methods) for the discretization of the Navier–Stokes equations is the simplicity of the algorithm and the computational efficiency. The LBM has been used mostly in the context of incompressible viscous Newtonian fluids [6]. Notable success of these 'minimal' LBM is, in particular, in the simulation of turbulent flows [7], time-dependent flows, flows in complex geometries [8–10] or flows through porous media [11, 12]. The kinetic nature of the LBM leads to the following features that distinguish the LBM from any other conventional CFD method [6, 13]. First, the convection operator of the LBM (or streaming process) is linear in phase space, similar to that of the Boltzmann kinetic equation but different from the one in the Navier–Stokes equations. Simple convection combined with a relaxation process (or collision operator) allows the recovery of the non-linear macroscopic advection through multi-scale expansions. Second, the pressure is obtained through an equation of state, as opposed to solving a Poisson equation in the incompressible Navier–Stokes equations. Solving the Poisson equation for the pressure often produces numerical difficulties requiring special treatment, such as iteration or relaxation. The incompressible Navier–Stokes equations can be obtained in the nearly incompressible limit of the LBM. Third, the LBM utilizes a minimal set of velocities in phase space. In the traditional kinetic theory with the Maxwell–Boltzmann equilibrium distribution, the phase space is a complete functional space. The averaging process involves information from the phase space. Because only one or two speeds and a few moving directions are used in LBM, the transformation relating the microscopic distribution function and macroscopic quantities is greatly simplified and consists of simple arithmetic calculations. Fourth, unlike the Navier–Stokes equations, in which macroscopic conservation laws are discretized, the LBM utilize a set of discrete particle velocities such that the conserved quantities are preserved up to machine accuracy in the calculations.

The objective of the present paper is to show that the LBM is able to produce results for the velocity, the shear stress and the first normal stress difference in the vicinity of the contraction in agreement with FVM simulations, which uses fully developed one-dimensional flow regions far up- and far downstream. For LBM approach, the stress field is directly obtained from the distribution function, while calculations of the stress based on the FVM-data use the evaluations of velocity gradients with finite differences. The shear stress and the first normal stress difference contain all the effects of deformation on a material. Thus, the stress field for both LBM and FVM is expressed in the present study in terms of the shear stress and the first normal stress difference.

This paper is organized as follows: Section 2 provides a brief introduction of the governing equations. Sections 3 and 4 introduce both LBM and FVM methods, respectively. Section 5 describes the flow system of a 2D symmetric channel with sudden contraction used in this study, and provides the details of the boundary conditions. Section 6 presents the numerical results and discussion of the LBM simulations, and the comparison with FVM results and analytical solutions when available. Section 7 concludes the paper and hints at work for future studies.

2. GOVERNING EQUATIONS

The motion of an isothermal fluids may be governed by conservation laws for mass and momentum. The continuity equation for incompressible fluids can be written as

$$\nabla \cdot \mathbf{v} = 0 \tag{1}$$

where $\mathbf{v}$ is the velocity. Incorporating conservative body forces into the hydrodynamic pressure, the conservation of momentum for steady state flows reads

$$\nabla \cdot (\rho \mathbf{v}\mathbf{v}) = -\nabla p + \nabla \cdot \boldsymbol{\tau} \tag{2}$$

where ρ is the density, p is the hydrodynamic pressure and $\boldsymbol{\tau}$ is the extra stress tensor. For an incompressible Newtonian fluid, the extra stress tensor $\boldsymbol{\tau}$ is given by

$$\boldsymbol{\tau} = 2\eta \mathbf{D} \tag{3}$$

where η is the fluid viscosity and $\mathbf{D}$ is the rate of strain tensor,

$$\mathbf{D} = \tfrac{1}{2}(\nabla \mathbf{v} + (\nabla \mathbf{v})^{\mathrm{T}}) \tag{4}$$

3. LATTICE-BOLTZMANN METHOD

The LBM[§] starts from a discrete distribution function $f_n(t, \mathbf{x}) \equiv f(t, \mathbf{x}, \mathbf{c}_n)$, where $\mathbf{c}_n$ is the discrete particle velocity. The function f_n leads to the mass density ρ and to the mass average velocity $\mathbf{v}$ via the identities [3]

$$\rho(t, \mathbf{x}) = \sum_n f_n(t, \mathbf{x}) \tag{5}$$

$$\rho \mathbf{v}(t, \mathbf{x}) = \sum_n \mathbf{c}_n f_n(t, \mathbf{x}) \tag{6}$$

The function f_n satisfies the hyperbolic equation

$$f_n(t+1, \mathbf{x} + \mathbf{c}_n) - f_n(t, \mathbf{x}) = -\frac{1}{\vartheta}(f_n(t, \mathbf{x}) - f_n^{\mathrm{eq}}(t, \mathbf{x})) \tag{7}$$

[§]In LBM units all quantities are dimensionless.

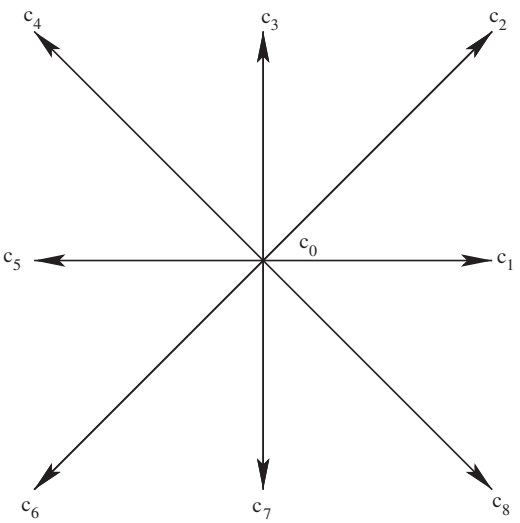

Figure 1. Nine-speed square lattice used in the LBM simulation carried out in this study.

where ϑ is a dimensionless collision frequency. Here, f_n^{eq} is the equilibrium distribution function given by [3]

$$f_n^{\mathrm{eq}} = w_n \rho (1 + 3(\mathbf{c}_n \cdot \mathbf{v}) + \tfrac{9}{2}(\mathbf{c}_n \cdot \mathbf{v})^2 - \tfrac{3}{2} v^2) \tag{8}$$

For two-dimensional problems with a square lattice ($\Delta x = \Delta y = 1$), it is customary to use nine discrete velocities (the D_2Q_9 scheme) shown in Figure 1

$$\begin{aligned} &\mathbf{c}_0 = 0 \\ &\mathbf{c}_n = \left(\cos\left(\frac{(n-1)\pi}{4}\right), \sin\left(\frac{(n-1)\pi}{4}\right)\right) \quad \text{for } n = 1,3,5,7 \\ &\mathbf{c}_n = \sqrt{2}\left(\cos\left(\frac{(n-1)\pi}{4}\right), \sin\left(\frac{(n-1)\pi}{4}\right)\right) \quad \text{for } n = 2,4,6,8 \end{aligned} \tag{9}$$

The weighting coefficients w_n needed to satisfy Equations (5) and (6) for f_n^{eq} turn out to be [3, 6]

$$\begin{aligned} &w_0 = \tfrac{4}{9} \\ &w_n = \tfrac{1}{9} \quad \text{for } n = 1,3,5,7 \\ &w_n = \tfrac{1}{36} \quad \text{for } n = 2,4,6,8 \end{aligned} \tag{10}$$

Note that Equation (10) requires that the equilibrium distribution function can be used in Equations (5) and (6).

It has been shown [14] that this approach leads to Equations (1) and (2) with τ given by

$$\tau = -\left(1 - \frac{1}{2\vartheta}\right)\sum_n \mathbf{c}_n \mathbf{c}_n (f_n - f_n^{\mathrm{eq}}) \tag{11}$$

If one utilizes a Chapman–Enskog expansion in Equation (7) (note that for infinite collision frequency, $f_n = f_n^{\mathrm{eq}}$ is bound to prevail), then Equation (11) can be cast into the form [6]

$$\tau = \nu(\nabla(\rho\mathbf{v}) + (\nabla(\rho\mathbf{v}))^{\mathrm{T}}) \tag{12}$$

with the dimensionless kinematic viscosity and speed of sound c_s given by

$$\nu = \tfrac{1}{3}(\vartheta - \tfrac{1}{2}) \tag{13}$$

$$c_s = \tfrac{1}{\sqrt{3}} \tag{14}$$

The LBM has good stability properties for $0 < \vartheta^{-1} < 2$ (sub-relaxation for $0 < \vartheta^{-1} < 1$ and over-relaxation for $1 < \vartheta^{-1} < 2$). Thus, positive shear viscosity and stable solutions of Equation (7) go hand in hand.

3.1. Computational lattice and method of solution

Simplicity in implementation for the hyperbolic Equation (7) has been used as an argument in favour of the LBM. The simplest 'stream-and-collide' D_2Q_9 algorithm with single time relaxation and a bounce-back boundary condition formulation is considered in this study. This algorithm is easier to program and to handle than the continuum CFD algorithms for solving the momentum equations. On every lattice node $\mathbf{x}$, a set of n real numbers, the particle density distributions f_n, is stored. The updating of the lattice consists of basically two steps: a streaming process, where the particle densities are shifted in discrete time steps $\Delta t = 1$ through the lattice along the connection lines in direction to their next neighboring nodes, and a relaxation step, where locally that part of a new particle distribution is computed which results from the equivalent to the Boltzmann collision integrals, right-hand side of Equation (7). For every time step, all quantities (velocity, density, pressure) can locally be computed in terms of averages of this density distribution and (for the viscosity) the relaxation parameter.

3.2. Boundary conditions

Wall boundary condition. At walls, a bounce-back scheme is used to obtain no-slip velocity conditions [15, 16]. By the so-called bounce-back scheme, particle distributions streaming to a wall node scatter back in the original direction. This guarantees that the no-slip condition is satisfied.

Inflow boundary condition. The velocity profile $u(y)$ as well as the density ρ of the fluid flow through a planar contraction investigated in this study are assigned at the inlet. A specified inlet velocity profile is easily implemented by constantly settling the inlet fields with the equilibrium population obtained from Equation (8). The inlet region was chosen to be long enough to ensure that a slight error which occurs when only the equilibrium distribution is taken into account has no influence on the results presented hereafter.

Outflow boundary condition. A zero gradient condition is set by simply copying the fields of the next to the last column into the last one, i.e. the outlet. This condition works well essentially if the outlet is located sufficiently far from the inlet. Otherwise, some numerical instabilities may appear.

Connection to real fluids. Since LBM uses only dimensionless quantities, dimensional reasoning is applied to obtain the connection to physical values. For Newtonian fluid, this is very simple and straight forward. Guaranteeing Reynolds number and geometry identities of LBM calculations and real physical systems imply identical dimensionless results. For the flow through a 4:1 planar contraction, the relation

$$\frac{\mathbf{v}}{u_\mathrm{o}} = \mathscr{F}\left(\frac{\mathbf{x}}{h}, \frac{h}{H}, Re\right) \tag{15}$$

will be hold. Here, u_o is the average outlet velocity and $\mathscr{F}$ is an arbitrary function. The dimensionless quantities of the relation are the ones calculated by LBM.

4. FINITE-VOLUME METHOD

To solve the non-linear coupled system of the conservation equations, Equations (1)–(3), we summarize the key features of the FVM used in this study. The flow domain is subdivided for a spatial discretization into a finite number of control volumes (CV), where the computational nodes are located at the centre of every CV. All variables are stored at the same grid node, i.e. a collocated arrangement is used. Due to the symmetry of the problem, only the upper half of the planar contraction geometry is resolved by an orthogonal, uniform grid. The governing equations can be written in terms of a general transport equation of the primitive variable ϕ:

$$\nabla \cdot (\rho \mathbf{v}\phi - \Gamma_\phi \nabla \phi) = S_\phi \tag{16}$$

where Γ_ϕ is the diffusion coefficient and S_ϕ is the source term. By integrating over each CV and applying of the Gauss theorem leads to

$$\int_A \mathbf{n} \cdot (\rho \mathbf{v}\phi - \Gamma_\phi \nabla \phi)\, \mathrm{d}A = \int_{\delta V} S_\phi \, \mathrm{d}V \tag{17}$$

where A is the surface area, $\mathbf{n}$ the normal unit vector of one CV face pointing outwards and δV is the volume of the CV. We assume that the values of the variables at the centre of the CV faces and at the centre of the CV are proper averages and thus prevail over the entire surface and the entire CV. Equation (17) can be written as

$$\sum_c \mathbf{n}_c \cdot (\rho \mathbf{v}\phi - \Gamma_\phi \nabla \phi)_c A_c = S_\phi \delta V \tag{18}$$

where the index c denotes the CV faces of one CV over which the summation is to be taken. At this point approximations have to be introduced since the values ϕ_c on the CV faces have to be determined by an appropriate interpolation scheme. The interpolation scheme relates the nodal value ϕ_P to its neighbouring CV values ϕ_nb. Substituting the discretized fluxes into Equation (18) yields an algebraic equation for every CV of the form

$$a_P \phi_P + \sum_\mathrm{nb} a_\mathrm{nb} \phi_\mathrm{nb} = S_P^\phi \tag{19}$$

For the entire solution domain thus results a matrix equation:

$$\mathbf{A} \cdot \mathbf{\Phi} = \mathbf{S} \tag{20}$$

where $\mathbf{A}$ is the penta-diagonal matrix of coefficients, $\mathbf{\Phi}$ is the solution vector of the unknown variables u, v and p and $\mathbf{S}$ is the source term vector. This equation is solved using the strongly implicit procedure (SIP), which is designed for algebraic equations that are discretization of partial differential equations. The method is based on the incomplete lower-upper (ILU) decomposition of the coefficient matrix $\mathbf{A}$ taking advantage of the sparseness of the matrix. In order to solve the coupled set of equations for u, v and p a pressure correction method is applied, namely the SIMPLE algorithm of Patankar and Spalding [17]. This process is repeated until the convergence criterion is reached, i.e. the sum of absolute residuals in all equations is reduced to some specified value, in our case 10^{-5}. Further technical details of this method may be found in Reference [18].

5. STATEMENT OF THE PROBLEM

The benchmark problem of flow through an abrupt 4:1 planar contraction with a reentrant corner for Newtonian as well as non-Newtonian fluids is known to be a good test case. Figure 2 shows a sketch of the flow geometry used in this study. A planar contraction geometry was used with an upstream height of $2H = 0.0256\,\text{m}$ and a downstream height of $2h = 0.0064\,\text{m}$. A Cartesian co-ordinate system is used with its origin in the contraction plane. A detailed study of the stress and velocity fields will be presented for the laminar flow at a Reynolds number of one, $Re = \rho u_o h/\eta = 1$, where ρ is the fluid density, u_o is the average outlet velocity and η is the viscosity. The lengths of the inlet and outlet channels were taken to be long enough, $30h$ in the upstream channel and $15h$ in the downstream section, to reach a fully developed flow far away from the contraction plane. Referring to Figure 2, the boundary conditions are no-slip condition on the walls. At the inlet a fully developed velocity profile is prescribed. At the outlet, which is located far downstream with respect to the region of interest of the flow, a Neumann boundary condition is applied. At the plane of symmetry the normal component of the velocity and the normal gradients of the tangential velocity are zero.

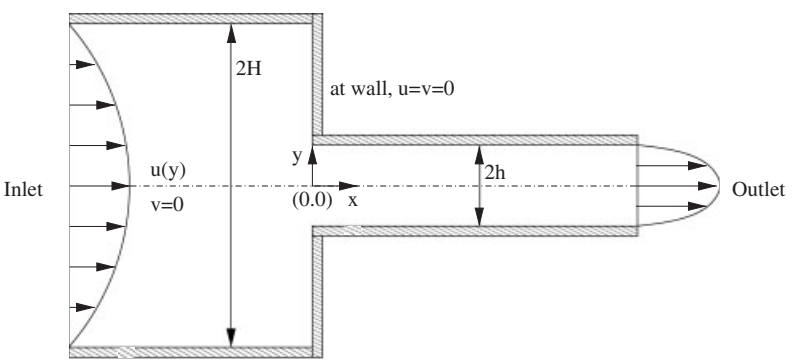

Figure 2. Sketch of the flow geometry with boundary conditions.

In order for a comparison with FVM simulation, it is necessary only to match the Reynolds number and geometry in the LBM simulation for fluid flow. The physical velocity and stress fields can be expressed in terms of dimensionless velocity and stress in the LBM calculations. To check the effect of grid refinement on the numerical results, two uniform grids (or lattice for LBM) were used for both numerical methods, LBM and FVM. The coarse grid/lattice consists of $1125 \cdot 200$ CVs (or nodes for LBM) in the x and y directions, respectively. The fine grid/lattice consists of $2250 \cdot 400$ CVs/nodes. The solutions obtained on both grids agree very well; thus the solutions may be regarded as grid converged and only the results of the fine grid/lattice are presented. In this study, the stress field for both LBM and FVM is expressed in terms of the shear stress τ_{xy} and the first normal stress difference $N1$, $N1 = \tau_{xx} - \tau_{yy}$. The calculations of the shear stress τ_{xy} and the first normal stress difference $N1$ based on the FVM-data use the evaluations of velocity gradients with finite differences, recall Equation (3). In the LBM approach, the stress components may be directly obtained from the distribution function according to Equation (11).

6. RESULTS AND DISCUSSION

The numerical results for the Newtonian fluid flow at Reynolds number $Re = 1$ will be presented in form of velocity and stress profiles upstream and downstream of the contraction as well as along the centreline. Profiles of the shear stress τ_{xy} and the first normal stress difference $N1$ are calculated from the completely converged flow kinematics. The numerical results for both τ_{xy} and $N1$ have been non-dimensionalized with respect to τ_o, which is given by

$$\tau_o = \eta\left(\frac{u_o}{h}\right) \tag{21}$$

6.1. Evaluation of the velocity distribution

6.1.1. Velocity profiles upstream of the contraction plane. Figure 3 displays the streamlines along the contraction for the LBM simulation, where a recirculation can be observed. Figure 4 shows the lateral profiles of the axial velocity u along x for the LBM simulation results. For more details, Figure 5 shows the upstream lateral profiles of the axial velocity u in front of the contraction for the LBM simulation as compared to FVM results. As expected from the theoretical analysis for Newtonian fluid flow between two parallel plates, the velocity profile far upstream of the contraction is parabolic, i.e. one-dimensional fully developed flow as assumed at the inlet. The velocity profiles in this region are in excellent agreement with the analytical solution for both methods, which is given by

$$\frac{u}{u_{avg}} = \frac{4u}{u_o} = 1.5\left(1 - \left(\frac{y}{4h}\right)^2\right) \tag{22}$$

where $u/u_{avg} = 1.5$ at the centreline $y/h = 0$. The area under each curve is the volumetric flow rate, which is constant as a result of the conservation law of mass. LBM predicts slightly larger velocity values compared to FVM in the core region of the flow when approaching the contraction. For $y/h > 1$, LBM predicts slightly lower velocity values compared to FVM so that the volumetric flow rate for each method is the same. Figure 6 shows the axial scans of the velocity profiles, where both numerical results are in excellent agreement with each other.

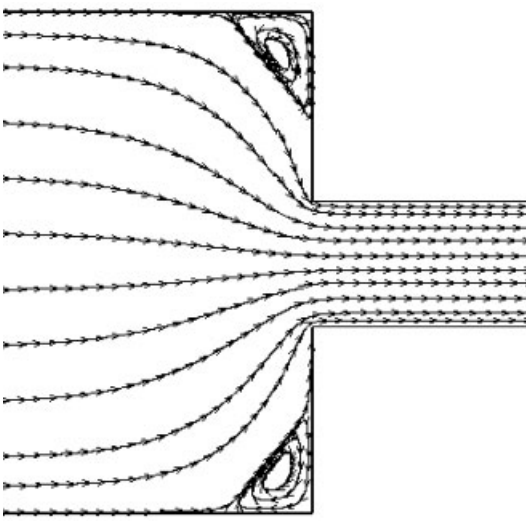

Figure 3. Streamlines along the contraction at $Re = 1$ for LBM simulation.

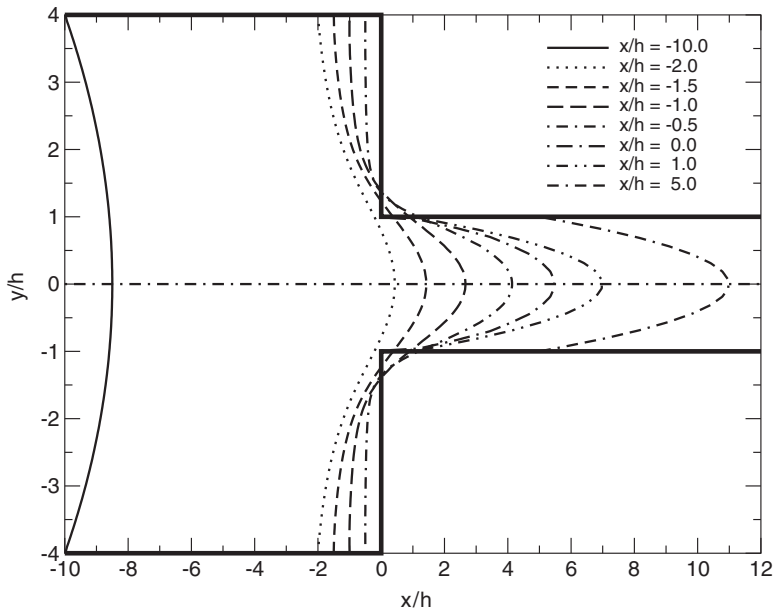

Figure 4. Lateral profiles of the velocity along the contraction for the LBM simulation.

6.1.2. Velocity profiles downstream of the contraction plane. Figure 7 presents the axial velocity profiles in the downstream section of the flow at $x/h = 0, 1, 5$. The profiles for both LBM and FVM methods show good agreement with each other. At $x/h > 1$ after the contraction,

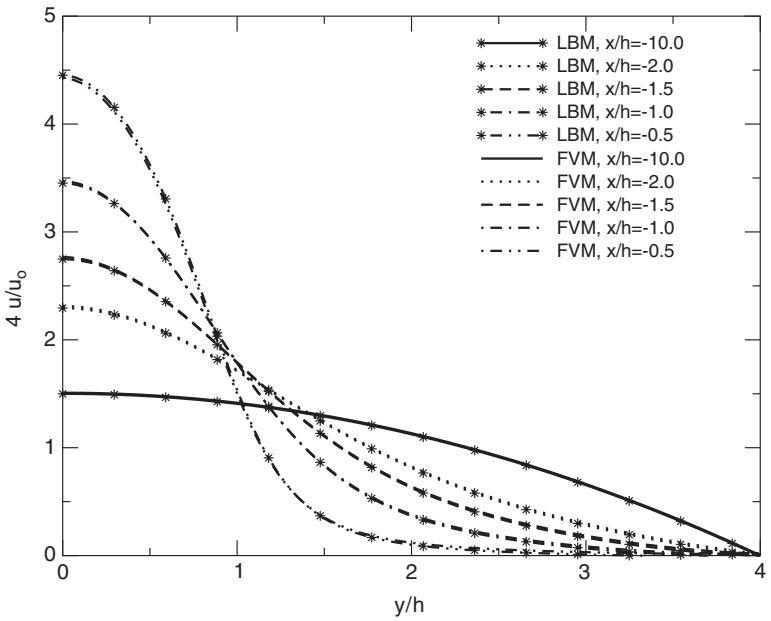

Figure 5. Lateral profiles of the velocity in upstream of the contraction for both LBM and FVM simulations.

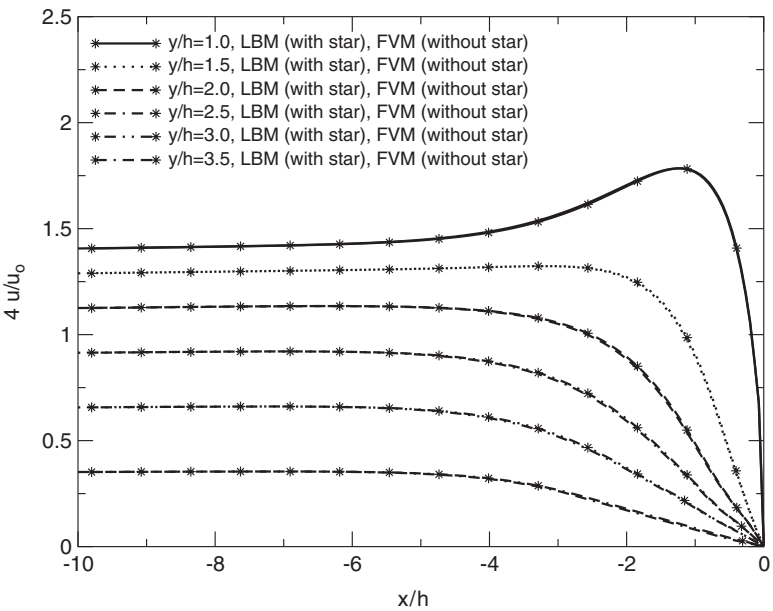

Figure 6. Axial scans of the velocity profiles in the upstream section of the channel for both LBM and FVM simulations.

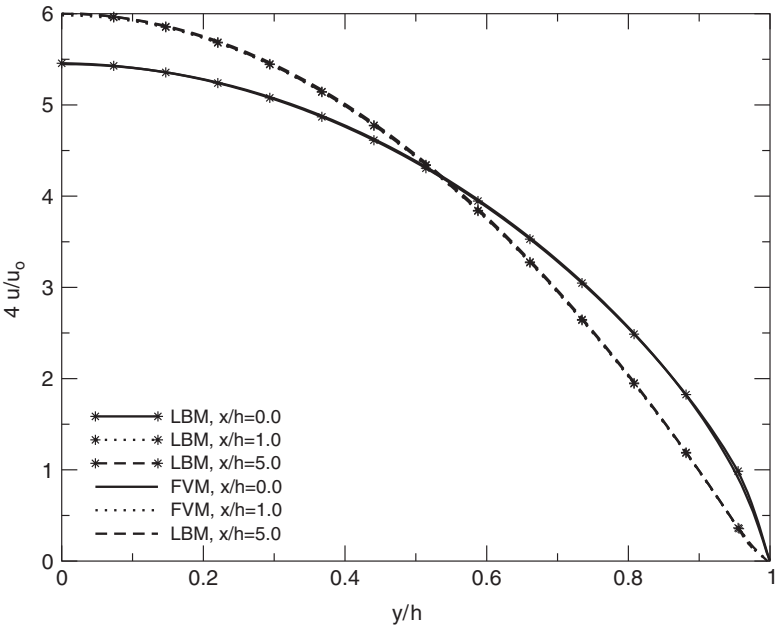

Figure 7. Lateral profiles of the velocity in the downstream section of the contraction for both LBM and FVM simulations.

the profile becomes parabolic and one-dimensional fully developed. The velocity profiles in this region are in excellent agreement for both methods with the analytical solution, which is given by

$$\frac{u}{4u_{\text{avg}}} = \frac{u}{u_{\text{o}}} = 1.5\left(1 - \left(\frac{y}{h}\right)^2\right) \tag{23}$$

where $u/u_{\text{avg}} = 6$ at the centreline of the 4:1 contraction.

6.1.3. Velocity profiles along the centreline and for $y/h = 0.5$. Figure 8 shows the centreline velocity and the velocity at $y/h = 0.5$ along the contraction for both LBM and FVM. Both numerical methods are in good agreement with each other. For the velocity at $y/h = 0.5$, a small velocity overshoot after the contraction can be observed for the simulations of both models.

6.2. Evaluation of the shear stress and the first normal stress difference

6.2.1. Shear stress and first normal stress difference profiles upstream of the contraction plane. Figure 9 shows the cross-sectional shear stress profiles upstream of the contraction. At $x/h = -10$ upstream of the contraction, where the flow is one-dimensional fully developed, the shear stress is a straight line with a slope $= -3/64$ for both LBM and FVM simulations.

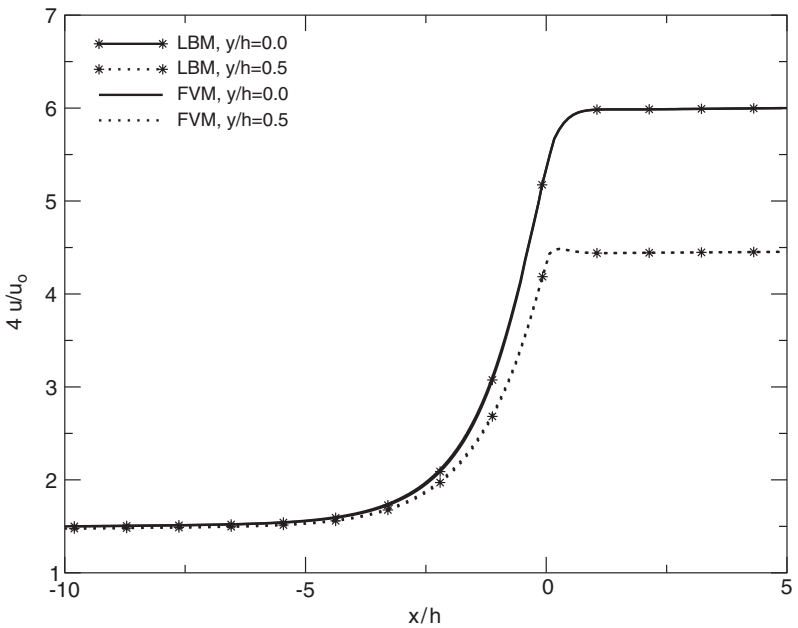

Figure 8. Velocity at different values of y/h along the contraction for both LBM and FVM.

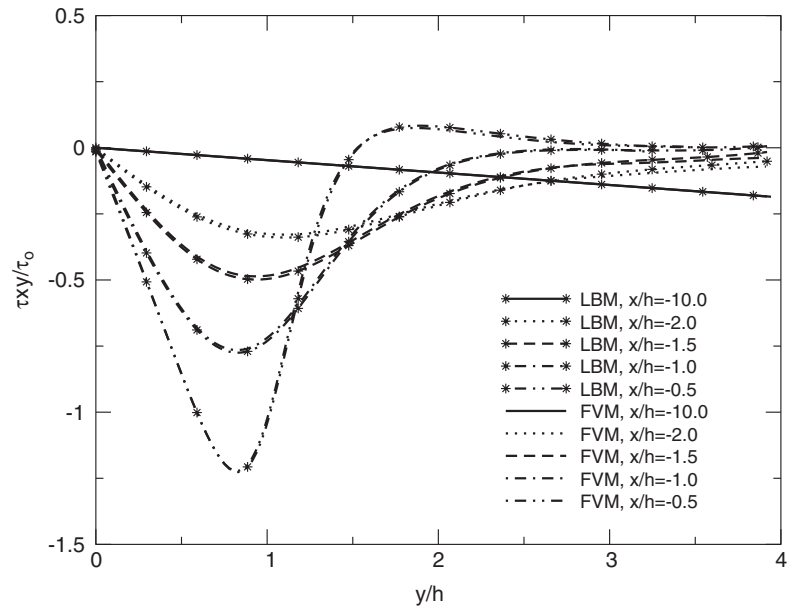

Figure 9. Lateral scans of the shear stress profiles in the upstream section of the channel for both LBM and FVM.

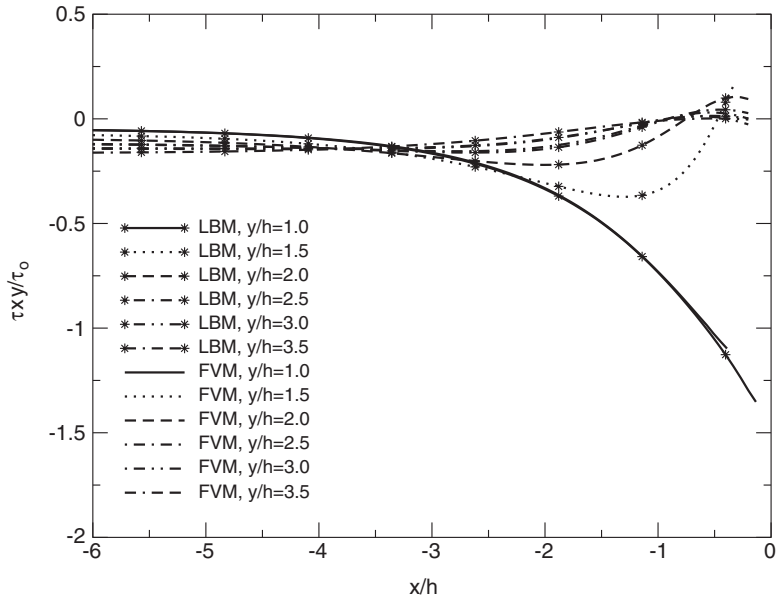

Figure 10. Axial scans of the shear stress profiles in the upstream section of the channel for both LBM and FVM.

The analytical solution for the shear stress in this region, one-dimensional fully developed, is a linear function of y, i.e.

$$\tau_{xy} = \eta\left(\frac{\mathrm{d}u}{\mathrm{d}y}\right) = -\left(\frac{3}{64}\,\frac{\eta u_{\mathrm{o}}}{h}\right)\left(\frac{y}{h}\right) \tag{24}$$

Figure 9 shows that simulated minima appear already at $y/h < 1$ for higher x/h values. The value of the maxima increases when approaching the contraction. Figure 10 shows the axial profiles of the shear stress in the upstream region. For $y/h = 1$ and $x/y \simeq 0$, the numerical results increase strongly as a result of the singularity at the corner. Figure 11 shows the lateral profiles of the first normal stress difference. It is clear that for a fully developed flow, $N1 = 0$, in agreement with the analytical solution,

$$\begin{aligned} N1 &= \tau_{xx} - \tau_{yy} \\ &= 2\eta\left(\frac{\partial u}{\partial x} - \frac{\partial v}{\partial y}\right) \\ &= 4\eta\left(\frac{\partial u}{\partial x}\right) \\ &= 0 \end{aligned} \tag{25}$$

For the two-dimensional flow, near the contraction, the peak values of the first normal stress difference is along the centreline. The value of the peak increases when approaching the

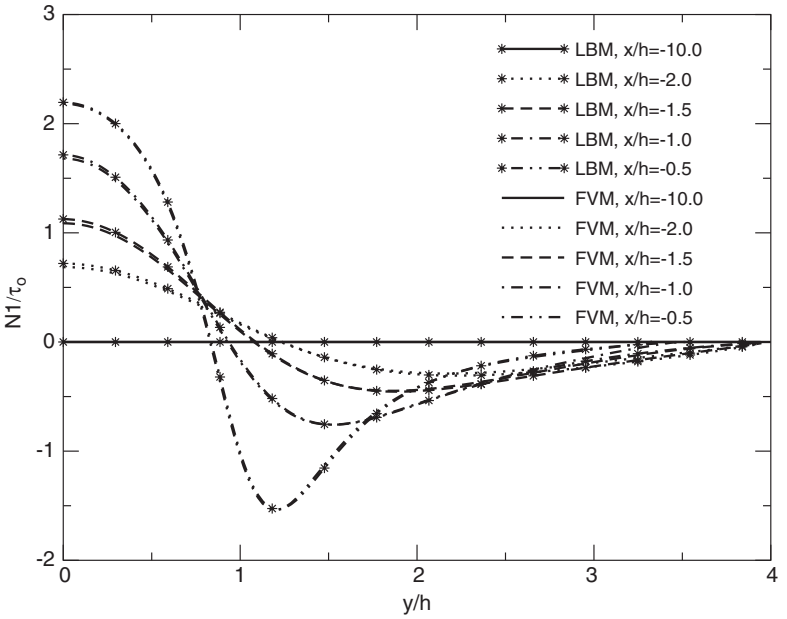

Figure 11. Lateral scans of the first normal stress difference profiles in the upstream section of the channel for both LBM and FVM.

contraction. The axial scans of the first normal stress difference profiles in the upstream section of the channel are shown in Figure 12. It is seen that both LBM and FVM simulations are in good agreement with each other, except close to the corner.

6.2.2. Shear stress and first normal stress difference profiles downstream of the contraction plane. The cross-sectional shear stress profiles after the contraction are shown in Figure 13. The analytical solution for the shear stress far downstream of the contraction in the one-dimensional fully developed flow region with respect to y/h is a straight line with a slope $= -3$, i.e.

$$\tau_{xy} = \eta\left(\frac{\mathrm{d}u}{\mathrm{d}y}\right) = -\left(3\,\frac{\eta u_{\mathrm{o}}}{h}\right)\left(\frac{y}{h}\right) \tag{26}$$

Figure 14 illustrates the behaviour of the lateral scans of the first normal stress difference in several x/h co-ordinates after the contraction. It is clear again that in the one-dimensional fully developed flow regions, far up- and far downstream of the contraction, $N1 = 0$, which is in agreement with the analytical solution, see Figure 16. Figures 13 and 14 show differences between LBM and FVM simulations close to the corner, as well as close to the wall. However, the flow at the sharp corner is singular [19, 20]. The singularity present at the sharp corner is responsible for many difficulties associated with the numerical simulations of fluid flows [21].

6.2.3. Shear stress and first normal stress difference profiles along the centreline and for $y/h = 0.5$. Figure 15 shows axial shear stress profiles at $y/h = 0$ and $y/h = 0.5$. The shear stress

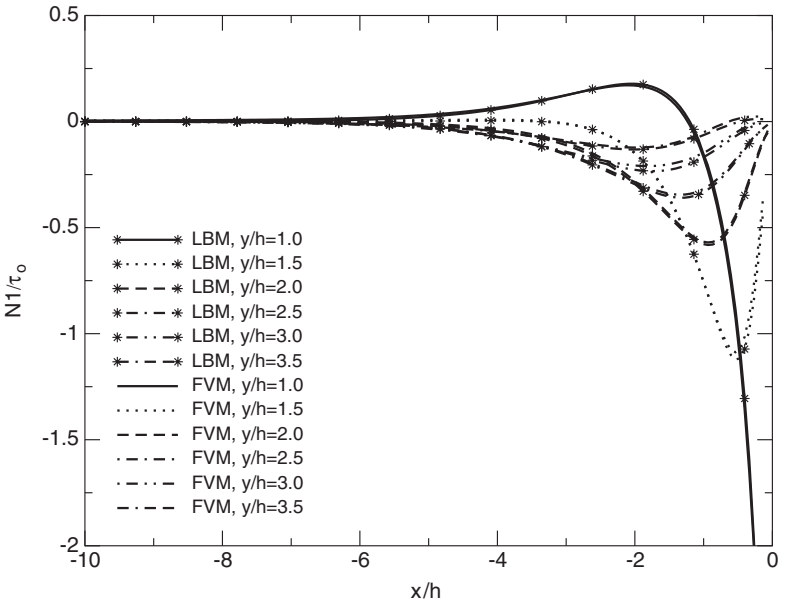

Figure 12. Axial scans of the first normal stress difference profiles in the upstream section of the channel for both LBM and FVM.

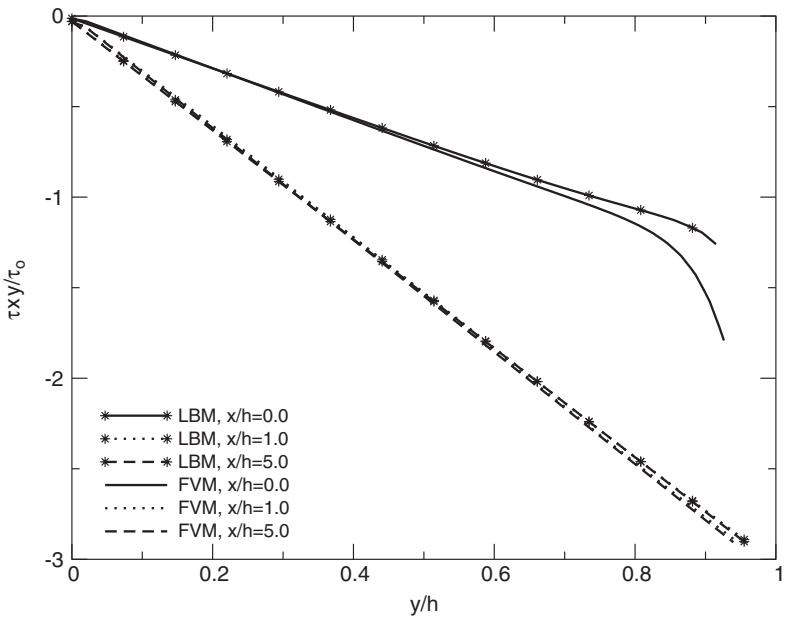

Figure 13. Lateral scans of the shear stress profiles in the downstream section of the contraction for both LBM and FVM.

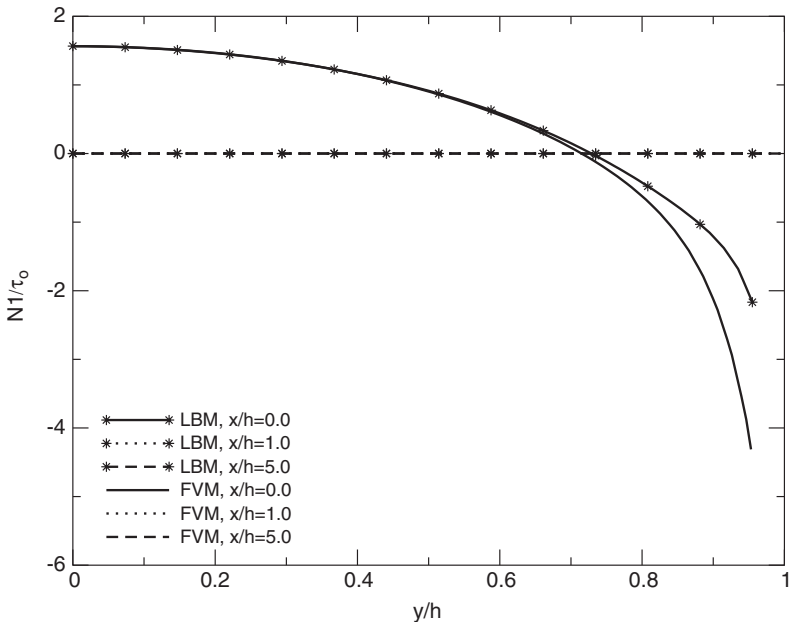

Figure 14. Lateral scans of the first normal stress difference profiles in the downstream section of the contraction for both LBM and FVM.

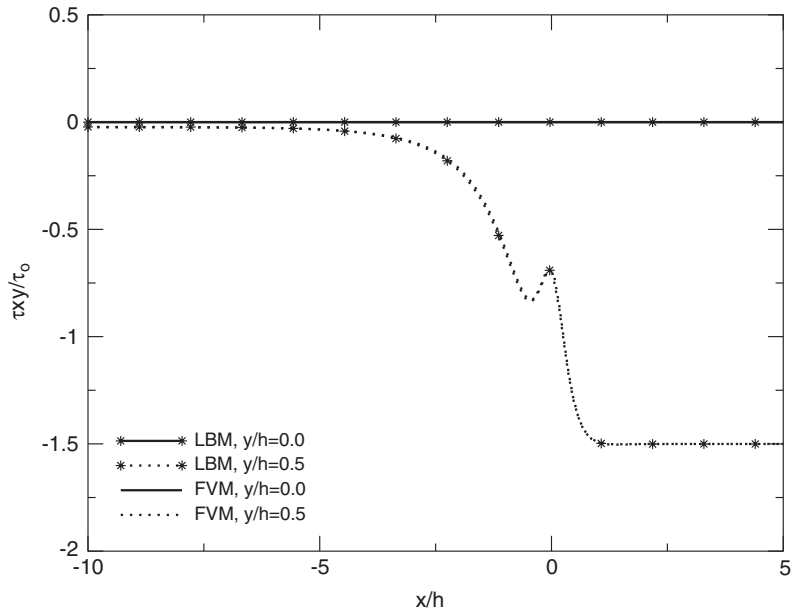

Figure 15. Shear stress profiles at different values of y/h for both LBM and FVM.

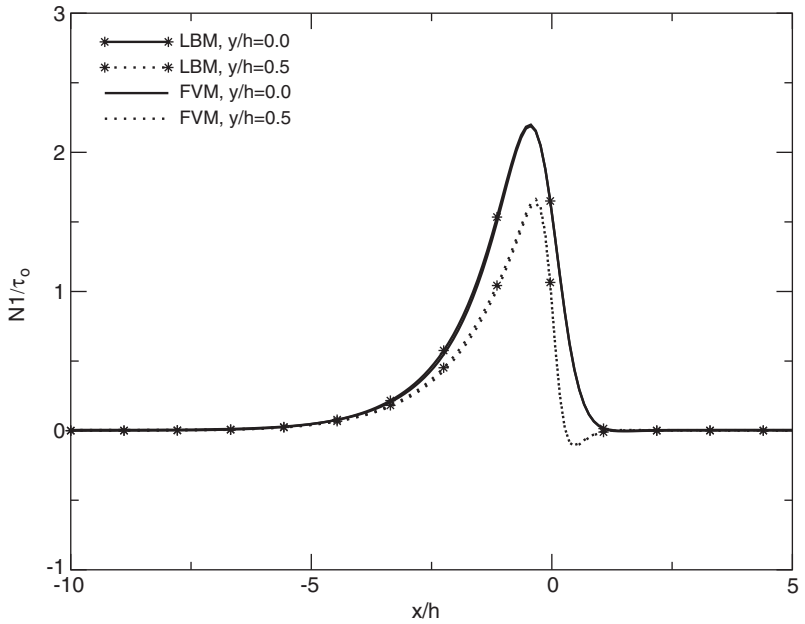

Figure 16. First normal stress difference profiles at different values of y/h for both LBM and FVM.

profiles along the centreline are zero as a result of the symmetry at $y/h = 0$. An overshoot in the shear stress upstream of the contraction can be also observed. Figure 16 shows a maximum value of the first normal stress difference slightly before approaching the contraction. This maximum value becomes lower by approaching the centreline, which is also the symmetry line. The velocity overshoot seen in Figure 8 leads to the negative $N1$ values shortly after the contraction,

$$N1 = \tau_{xx} - \tau_{yy} = 4\eta\left(\frac{\partial u}{\partial x}\right) \tag{27}$$

The comparison of the analytical results and the data obtained with LBM and FVM clearly verify the numerical methods. Though the resolution of the computational grids was quite coarse in the vicinity of the corner, reasonable agreement was obtained. However, to obtain hopefully better agreement local refinement of the computational meshes close to the singular corner are required. This will be the subject of the next chapter.

7. SUMMARY AND CONCLUSIONS

In this study, we conducted for the velocity field a comparison of both LBM and FVM for the numerical simulation of Newtonian fluid through a planar 4:1 contraction. The lateral and axial profiles of the velocity were compared. Using both LBM and FVM, the shear stress and the first normal stress difference were studied in detail for the Reynolds number one. The velocity profiles of both LBM and FVM are in excellent agreement with each other and with

the analytical solution in the one-dimensional fully developed flow regions. The shear stress and the first normal stress difference are also investigated. The numerical simulations for both LBM and FVM are in agreement with each other away from the corner. Numerical simulations for both LBM and FVM are in agreement with the analytical solution when available. The lattice-Boltzmann method (LBM) is an alternative and promising way in simulating Newtonian fluid flows through contraction or even more complex geometries. The advantage of the LBM compared to the 'classical' finite volume method for the discretization of the Navier–Stokes equations is the simplicity of the algorithm and the computational efficiency.

ACKNOWLEDGEMENT

The present work was funded in part by the German Academic Exchange Service, DAAD, under an individual grant. This is gratefully acknowledged.

REFERENCES

1. McNamara G, Zanetti G. Use of Boltzmann equation to simulate lattice gas automata. *Physics Review Letters* 1988; **61**:2332–2335.
2. Higuera F, Jimenez J. Lattice gas dynamics with enhanced collision. *Europhysics Letters* 1989; **9**:663–668.
3. Qian Y, d'Humieres D, Lallemand P. Lattice BGK models for Navier–Stokes equation. *Europhysics Letters* 1992; **17**(6):479–484.
4. Bhatnagar P, Gross E, Krook M. A model for collision processes in gases. I: Small amplitude processes in charged and neutral one-component system. *Physical Review* 1954; **94**:511–525.
5. Chen H, Chen S, Matthaeus W. Recovery of the Navier–Stokes equation using a lattice Boltzmann method. *Physical Review A* 1991; **45**:5339–5342.
6. Chen S, Doolen G. Lattice Boltzmann method for fluid flows. *Annual Review of Fluid Mechanics* 1998; **30**: 329–364.
7. Toschi F, Amati G, Succi S, Benzi R, Piva R. Intermittency and structure functions in channel flow turbulence. *Physics Review Letters* 1999; **82**:5044–5047.
8. Hou S, Doolen G, Zou Q, Chen S, Cogley A. Simulation of cavity flow by the lattice Boltzmann method. *Journal of Computational Physics* 1995; **118**:329–347.
9. Brenner G, Zeiser T, Lammers P, Bernsdorf J, Durst F. Applications of lattice Boltzmann methods in CFD. *ERCOFTAC Bulletin* 2001; **50**:29–34.
10. Freund H, Zeiser T, Huber F, Klemm E, Brenner G, Durst F, Emig G. Numerical simulations of single phase reacting flows in randomly packed fixed-bed reactors and experimental validation. *Chemical Engineering Science* 2003; **58**:903–910.
11. Buckles J, Hazlett R, Chen S, Eggert K, Grunau D, Soll W. Flow through porous media using lattice Boltzmann method. *Los Alamos Science* 1994; **22**:112–121.
12. Martys N, Chen H. Simulation of multicomponent fluids in complex three-dimensional geometries by the lattice Boltzmann method. *Physical Review* 1994; E**53**:743–750.
13. Lockard D, Luo L-S, Milder S, Singer B. Evaluation of PowerFLOW for aerodynamic applications. *Journal of Statistical Physics* 2002; **107**(1/2):423–478.
14. Krafczyk M. Gitter Boltzmann Methoden: Von der Theorie zur Anwendung. *State Doctorate Thesis*, Technical University of Munich, Germany, 2001.
15. Wolfram S. Cellular automaton fluids. 1: Basic theory. *Journal of Statistical Physics* 1986; **45**:471–526.
16. Lavallée P, Boon JP, Noullez A. Boundaries in lattice gas flows. *Physica D* 1991; **47**:233–240.
17. Patankar S, Spalding D. A calculation procedure for heat, mass and momentum transfer in three-dimensional parabolic flows. *International Journal of Heat and Mass Transfer* 1972; **15**:1787–1806.
18. Ferziger J, Peric M. *Computational Methods for Fluid Dynamics*. Springer: Berlin, 1996.
19. Moffatt H. Viscous and resistive eddies near a sharp corner. *Journal of Fluid Mechanics* 1964; **18**:1–18.
20. Crochet M, Davies A, Walters K. *Numerical Simulation of Non-Newtonian Flow*. Elsevier: Netherlands, 1984.
21. Mompean G. On predicting abrupt contraction flows with differential and algebraic viscoelastic models. *Computers and Fluids* 2002; **31**:935–956.

